Optimal Longitudinal Trajectories for Reusable Space Vehicles in the Terminal Area

S. De Ridder* and E. Mooij[†]

Delft University of Technology, 2629 HS Delft, The Netherlands

This paper concerns optimal longitudinal trajectories and guidance strategies of a reusable launch vehicle during the terminal-area energy-management phase. During this phase, it is important to know the limits of the vehicle capabilities and the best strategy for a flight in the vertical plane. This paper describes optimal trajectories using a genetic algorithm and guidance strategies for both maximum-range and maximum-dive flights. The optimal trajectories show an increased maximum range up to 6%, compared with the trajectories using an angle of attack for maximum lift-to-drag ratio. A turning flight has an influence on the optimal trajectories and optimal turns are flown at a lower velocity. Based on the calculation of optimal trajectories and an energy-state approximation analysis, a longitudinal guidance law is designed, using robust design to approximate the optimal trajectories. Offnominal conditions, in terms of a change in initial altitude and velocity, also have an influence on the optimal trajectories. Maximum-range trajectories for different initial states define the minimum-energy boundary in the energy space.

Nomenclature

a	=	speed of sound, m/s
C_D	=	drag force coefficient,
C_L	=	lift force coefficient,
D	=	drag force, N
E_h	=	energy height, m
E_{kin}	=	kinetic energy, J
E_{pot}	=	potential energy, J
E_{tot}	=	total energy, J
g	=	Earth's gravitational acceleration, m/s^2
h	=	altitude, m
L	=	lift force, N
M	=	Mach number,
m	=	vehicle mass, kg
$\bar{q}$	=	dynamic pressure, Pa
R	=	heading alignment cylinder radius, m
r	=	radial distance from Earth's center to the vehicle, m
S_{ref}	=	aerodynamic reference area, m^2
s	=	glide range, m
V	=	airspeed, m/s
x	=	downrange along runway centerline, m
y	=	cross range with respect to runway centerline, m
α	=	angle of attack, rad
γ	=	flight-path angle, rad
δ	=	latitude, rad
ρ	=	atmospheric density, kg/m^3
σ	=	bank angle, rad
τ	=	longitude, rad
χ	=	heading angle, rad
ω	=	Earth rotation, rad/s

*M.Sc. Student; currently Research Engineer, Royal Military Academy, Electrical Engineering Department, Belgium; sven.de.ridder@elec.rma.ac.be.

[†]Assistant Professor, Astrodynamics and Space Missions, Faculty of Aerospace Engineering, Kluyverweg 1; e.mooij@tudelft.nl. Senior Member AIAA.
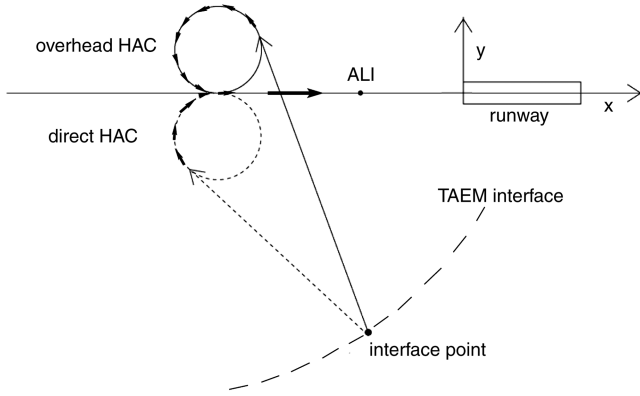
I. Introduction

LAUNCH vehicles are indispensable in space flight and space exploration. Nowadays, launching payload or humans into space with the current expendable and semireusable launch vehicles is very expensive and highly inflexible. To reduce the costs of space transportation and to increase the flexibility (hence increasing the number of flights or frequency of flights), advanced fully reusable launch vehicles have to be designed [1–3]. Efforts continue to design such reusable launch vehicles for both government-funded and commercial (e.g., space tourism) applications. Objectives of these new reusable launchers include significant improvements in vehicle safety, reliability, and operational costs. Perhaps the most important goal is to reduce the probability of a catastrophic failure. Advanced guidance and control technologies will greatly improve the overall safety and reliability of future reusable launch vehicles [4] particularly during reentry.

The unpowered entry of a winged or lift-producing reentry vehicle, based on the successful shuttle reentry technique, consists of an atmospheric entry phase, a terminal-area energy-management (TAEM) phase, and an approach and landing phase [5]. The atmospheric entry usually starts at an altitude of 120 km and is characterized by a high heating rate, and the approach and landing phase is responsible for the final part of the runway approach and the actual landing. The focus in this paper will be on the TAEM phase, which is a critical flight phase that brings the unpowered winged reentry vehicle from the end of the atmospheric entry phase at about 25 km altitude and a Mach number of 2.5 to the approach and landing interface (ALI). The TAEM guidance must guide the vehicle to this interface, control the energy of the vehicle and align the vehicle with the runway heading. The most characteristic feature of the TAEM phase is the heading alignment cylinder (HAC; see Fig. 1). This imaginary cylinder tangentially touches the extension of the runway centerline, and the vehicle performs a turn around the surface of this cylinder to get aligned with the centerline. During the TAEM phase, the energy is regulated such that the vehicle will arrive at the HAC and at the ALI with the correct amount of energy. The key item in the TAEM phase, i.e., the correct control of the energy dissipation with respect to range, depends on the flying capabilities of the vehicle. The capabilities of the vehicle are bounded by the minimum and maximum amounts of energy that can be dissipated with respect to range. This corresponds with the maximum range and the maximum dive that the vehicle can perform, respectively.

Currently, the only reentry vehicle that uses a TAEM guidance system is the space shuttle. It relies on reference trajectories and tracking algorithms [5]. The reference trajectories are calculated before the flight and stored in the onboard computer. Several

Fig. 1 TAEM guidance phase.

reference trajectories must be stored to cope with changing flight situations, and hence a disadvantage of this method is that it requires extensive premission planning to account for all expected variations. However, since there is no onboard replanning, there is only limited flexibility to account for unexpected variations, which makes the system less robust.

To solve these problems, several terminal-area guidance studies [6,7] have investigated the use of onboard trajectory calculation or energy estimation to safely and reliably deliver a reusable launch vehicle to the proper ALI for a wide range of initial conditions and in the presence of environmental and vehicular uncertainties. In this paper, the focus will be on the ability to cope with offnominal conditions in terms of a different initial (i.e., at entry/TAEM interface) position and velocity. Most studies focus on changing only the lateral flight path (i.e., azimuth or heading). The current paper, however, concentrates on the longitudinal flight path. Thus, the products and theories of this paper could be used in designing longitudinal onboard guidance approaches to combine with external lateral guidance techniques.

As a longitudinal strategy, several current explicit reference-trajectory-based systems use a fixed predetermined longitudinal profile, i.e., dynamic pressure as a function of altitude [7–9]. In [10], a constant minimum-dynamic-pressure value is used. A tracking algorithm tracks the dynamic pressure profile or constant value. These nominal dynamic pressure profiles are selected such that they lie between the vehicle's maximum-glide and maximum-dive capabilities, i.e., the vertical corridor [7–9]. The vertical corridor and the nominal dynamic pressure profile are calculated for a single specific initial state and for a straight flight. However, these fixed vertical profiles are also used during a turning flight. The optimal maximum-range and maximum-dive trajectories, and hence the nominal trajectory, might differ for different initial states and in the case of a turning flight.

Another type of guidance, a predicting-capabilities-based system, is used in [11]. The required energy to reach the runway is continuously calculated, and the proper commands are calculated for dissipating or economizing energy. The energy excess is calculated by an energy estimator, which is based on a closed-form approximation. This analytical approximation is relatively accurate at subsonic velocities, but significant errors can occur at supersonic and transonic velocities [11]. Hence, the estimation must be improved, e.g., by using a numerical estimation.

This paper aims at characterizing optimal longitudinal trajectories and longitudinal guidance strategies in the terminal area of a reusable launch vehicle. The following questions will be addressed:

1) What are the optimal trajectories to perform a maximum-range and a maximum-dive flight?

2) What is the influence of variations in the initial altitude and velocity in these trajectories?

3) What is the influence of a turning flight on these trajectories?

4) What is the minimum energy required to fly a specific distance?

5) What is the influence of a change in initial position and velocity on this minimum?

It is noted that currently only changes in the initial state are considered. Other dispersions, such as atmospheric or aerodynamic uncertainties, should ultimately be investigated but were not included for this study.

To this end, Sec. II describes the models used, followed in Sec. III by the calculation of optimal maximum-range trajectories using a genetic algorithm. Also in this section, the optimal trajectories are compared with two common approximations, i.e., the quasi-steady-state and the energy-state approximations. At the end of this section, the minimum-energy boundary is discussed. Section IV describes the optimal maximum-dive trajectories, and in Sec. V, the influence of a turn on the optimal trajectories is investigated. Based on the information obtained in these sections (sub)optimal guidance laws are designed in Sec. VI. Finally, Sec. VII concludes this paper.

II. Model Description

A. Equations of Motion

For performance prediction of the longitudinal range, a point-mass model for the motion in the vertical plane would be adequate. However, since we will also study the influence of a turn on the optimal trajectories (Sec. V), we need a set of equations that describes the full 3-D motion. In this study, the equations of motion for an oblate Earth (rotating with an angular velocity ω) and assuming a central gravity field are used to simulate and calculate an optimal TAEM trajectory. In this model, position and velocity of the vehicle are defined in spherical coordinates: notably, the distance r, longitude τ, latitude δ, ground velocity V, flight-path angle γ, and heading χ [12,13]:

$$\dot{V} = -\frac{D}{m} - g \sin \gamma + \omega^2 r \cos \delta (\sin \gamma \cos \delta - \cos \gamma \sin \delta \cos \chi) \tag{1}$$

$$V\dot{\gamma} = \frac{L \cos \sigma}{m} - g \cos \gamma + 2\omega V \cos \delta \sin \chi + \frac{V^2}{r} \cos \gamma \\ + \omega^2 r \cos \delta (\cos \delta \cos \gamma + \sin \gamma \sin \delta \cos \chi) \tag{2}$$

$$V \cos \gamma \dot{\chi} = \frac{L \sin \sigma}{m} + 2\omega V (\sin \delta \cos \gamma - \cos \delta \sin \gamma \cos \chi) \\ + \frac{V^2}{r} \cos^2 \gamma \tan \delta \sin \chi + \omega^2 r \cos \delta \sin \delta \sin \chi \tag{3}$$

$$\dot{r} = \dot{h} = V \sin \gamma \tag{4}$$

$$\dot{\tau} = \frac{V \sin \chi \cos \gamma}{r \cos \delta} \tag{5}$$

$$\dot{\delta} = \frac{V \cos \chi \cos \gamma}{r} \tag{6}$$

In the above equations m is the vehicle mass, g is the gravitational acceleration, and σ is the bank angle, one of the two guidance parameters (with the angle of attack α being the other one). The aerodynamic forces (lift L and drag D) are defined as

$$L = C_L \bar{q} S_{\text{ref}} \tag{7}$$

$$D = C_D \bar{q} S_{\text{ref}} \tag{8}$$

with the dynamic pressure defined as $\bar{q} = \frac{1}{2} \rho V^2$. The aerodynamic lift and drag coefficients C_L and C_D are not constant, but depend on the vehicle configuration, control surface deflections, Mach number, Reynolds number, attitude of the vehicle (the angle of attack), and the altitude h [14]. The Mach number is defined as $M = V/a$, where a is the local speed of sound. The atmospheric properties are calculated using the U.S. Standard Atmosphere 1976. During this study, no wind was taken into account.

B. High-Orbit Ultraviolet-Visible Satellite Vehicle Model

The TAEM trajectories are calculated for a reference vehicle similar to the space shuttle, the High-Orbit Ultraviolet-Visible Satellite (HORUS-2B) [12,14], which is representative of the reusable concepts that are commonly studied. Initially foreseen as a fully reusable second stage to the Ariane-5 launcher, HORUS was unpowered, although it had been equipped with a deorbit engine and attitude control thrusters. Later, a rocket engine was added to the design, which then became the manned second stage of Sänger, the German two-stage-to-orbit reference concept. In this study, use has been made of the original design being that of an unpowered winged reentry vehicle, as shown in Fig. 2. The vehicle has a total length of 25.0 m, a wingspan of 13.0 m and a reentry mass of 26,029 kg. The subsonic and supersonic maximum L/D are equal to 4.0 and 2.3, respectively.

For attitude control, HORUS is equipped with both a reaction control system and aerodynamic control surfaces. Only the control surfaces are used during the terminal-area phase. The control surfaces include two rudders (deflection angles are positive outboard), two wing flaps or elevons (positive down) that can be operated as elevators (symmetric deflection) or ailerons (asymmetric deflection), and one body flap (positive down). The rudders are outward-movable only, which means that for yaw control only one rudder is active at a time. The rudders can also be used as speed brakes by simultaneously deflecting them.

In the case of a trajectory simulation, the actual aerodynamic coefficients are computed by table lookup with the angle of attack and the Mach number as the independent variables. The aerodynamic database includes an additional drag coefficient when the altitude is lower than 20 km to take the changing density into account. The speed brakes are modeled as an aerodynamic drag increment.

III. Maximum-Range Trajectories in the Vertical Plane

In the current study, optimal trajectories in the vertical plane are calculated using a genetic algorithm. Before discussing the optimization results, two common approximations to the maximum-range problem, a quasi-steady-state and an energy-state approximation, will be discussed. A comparison is made between these approximations and the real optimal trajectories. At the end of this section, the minimum-energy boundary is discussed.

A. Quasi-Steady-State Approximation

In the quasi-steady-state approximation, the accelerations are neglected and a steady flight is assumed in the longitudinal plane. Such an instantaneous steady flight condition occurs when the longitudinal velocity does not change, either in magnitude or in direction. To derive the corresponding equations we start from Eqs. (1–6) and assume a flat, nonrotating Earth. In this case, the dynamic equations simplify to

$$\dot{V} = -\frac{D}{m} - g \sin \gamma \tag{9}$$

$$V\dot{\gamma} = \frac{L \cos \sigma}{m} - g \cos \gamma \tag{10}$$

$$V\dot{\chi} = \frac{L \sin \sigma}{m \cos \gamma} \tag{11}$$

This yields the equilibrium force equations for a stationary glide:

$$-D - mg \sin \gamma = 0 \tag{12}$$

$$L \cos \sigma - mg \cos \gamma = 0 \tag{13}$$

$$\frac{L \sin \sigma}{m \cos \gamma} = V\dot{\chi} \tag{14}$$

The airspeed in a stationary glide is obtained by substituting Eq. (7) in Eq. (13):

$$V = \sqrt{\frac{mg}{S_{\text{ref}}} \frac{2}{\rho} \frac{1}{C_L} \frac{\cos \gamma}{\cos \sigma}} \tag{15}$$

Dividing Eq. (12) by Eq. (13) and substituting Eqs. (7) and (8) gives an expression for the equilibrium flight-path angle:

$$-\tan \gamma = \frac{C_D}{C_L} \frac{1}{\cos \sigma} \tag{16}$$

In Sec. V, an optimal-turning flight around the HAC is studied, which requires the $\cos \sigma$ term. However, in the current section, only a wings-level ($0°$ bank angle) motion in the vertical plane is considered. Hence, Eq. (14) can be discarded and the terms containing the bank angle in Eqs. (15) and (16) can be removed, as $\cos \sigma$ equals 1.

The fundamental tool used in the steady-state glide theory is the performance curve or the velocity polar. This curve tells us the rate of descent of the vehicle at each horizontal velocity. The length of a vector from the origin to a point on the performance curve represents the magnitude of the airspeed along the flight path, and the angle
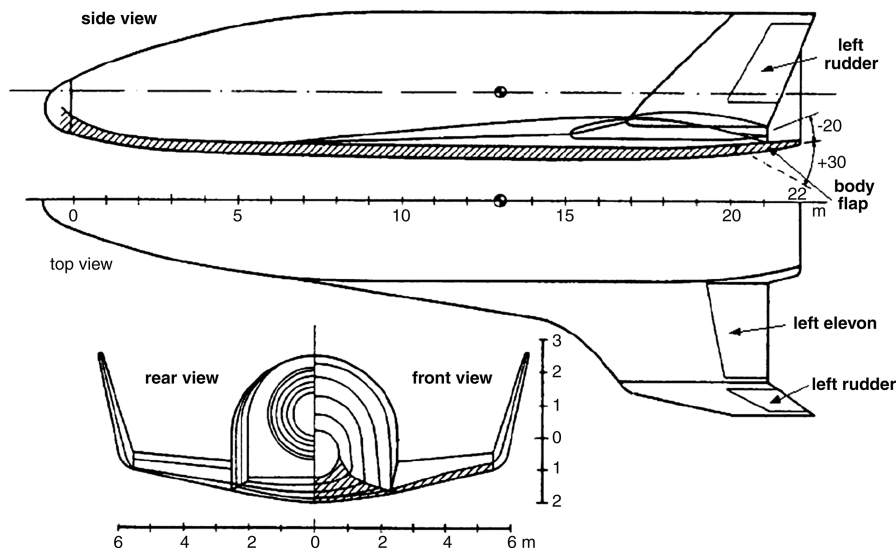

Fig. 2 Unpowered HORUS-2B reference vehicle [12].

confined between the horizontal axis and the velocity vector is the flight-path angle. Because of changing density, altitude has an effect on the performance curve. The performance curves can be calculated by using the equations stated above in an iteration process. The required steps to calculate a single point on the performance curve are as follows:

1) Specify the velocity, V_{req}, for which it is required to calculate the horizontal component and the vertical component (rate of descent) during steady state.

2) Calculate corresponding Mach number at the specified altitude.

3) Specify an initial guess for the angle of attack.

4) Calculate lift and drag coefficients using the aerodynamic model. C_D and C_L depends on the angle of attack and the Mach number.

5) Calculate γ using Eq. (16).

6) Calculate V using Eq. (15).

7) Compare V with V_{req}.

8) Update the guess for the angle of attack and repeat steps 4, 5, 6, and 7 until the difference $|V - V_{req}|$ is small enough.

9) When $V \approx V_{req}$, the converged values for α and γ are found, corresponding to a steady state at V_{req} and a specified altitude. Using the obtained γ, the horizontal and vertical velocity components are computed.

Repeating this process for several velocities between the stall speed and the maximum velocity yields the complete performance curve for a specific altitude. The maximum velocity follows from the $\bar{q}_{max}$ constraint, evaluated at the specified altitude. Figure 3 shows the calculated performance curves for several altitudes. Each point on a performance curve corresponds to equilibrium glide conditions for a constant angle of attack at the specified altitude. Along the performance curve, the angle of attack is changing.

In a steady glide, the maximum range is flown with a maximum ratio between the horizontal velocity and the negative of the rate of descent. This corresponds with a minimum-magnitude (i.e., shallowest) flight-path angle, which is obtained by drawing a tangent from the origin to the performance curve. This tangent point is the steady maximum-range point. Using Eq. (16), the requirement of minimum flight-path angle can be translated into a maximum lift-to-drag ratio L/D. Hence, a common interpretation of the steady-state approximation is to construct an angle-of-attack profile for a maximum L/D as a function of velocity or Mach number and to use this profile to calculate the maximum range [7,8]. The corresponding angle-of-attack profile for HORUS is shown in Fig. 4. It is noted that due to trim limitations HORUS cannot fly with the angle of attack for a maximum L/D in the transonic flow regime.

Using this angle-of-attack profile, the range was calculated for three subsonic and three supersonic initial conditions by propagating the trajectory. The three subsonic initial conditions all have an identical initial energy, but with a different distribution of kinetic and potential energy, i.e., a different combination of altitude and velocity. The same holds for the three supersonic points. The initial flight-path angle for subsonic initial conditions is the flight-path angle required for a steady-state glide at the initial velocity, and the initial flight-path angle for supersonic initial conditions is set to $-10°$, in order to match the flight-path angle at the end of the hypersonic descent [12]. The initial conditions and the corresponding ranges using $\alpha_{(L/D)\,max}$
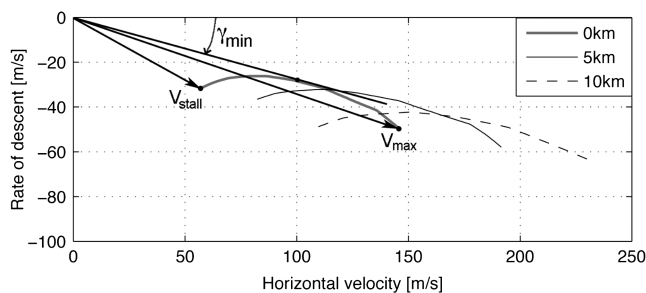

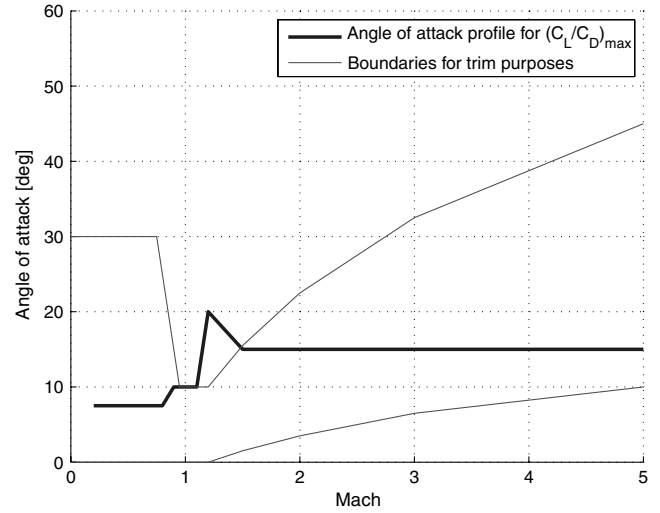Fig. 3 Performance curves of HORUS for different altitudes.

Fig. 4 Angle-of-attack profile for maximum L/D and α boundaries as a function of Mach number.

are given in Table 1. The initial energy is commonly defined as an energy height, derived from the definition of total mechanical energy:

$$E_{tot} = mgh + \tfrac{1}{2}mV^2 \qquad (17)$$

Assuming a constant gravity field, an expression for the specific energy or *energy height* is obtained, which is defined as the total energy divided by the weight:

$$E_h = \frac{E}{mg_0} = h + \frac{1}{2g_0}V^2 \qquad (18)$$

As an alternative to flying at maximum L/D, another interpretation of the steady-state approximation is to fly at a constant dynamic pressure. A stated before, altitude has an effect on the performance curve. The lower the density, the faster the vehicle flies and sinks, but the ratio between the velocity and the sink rate remains the same. Using Eq. (15), inserting a constant flight-path angle (steady-state) and assuming a constant lift coefficient gives a relation between the glide velocity for a steady-state flight at altitude h_1 and at sea level h_0:

$$\frac{V_{h1}}{V_{h0}} = \sqrt{\frac{\rho_0}{\rho_1}} \qquad (19)$$

This equation shows that a maximum-range flight, assuming steady-state glide and constant aerodynamics, requires that the vehicle is controlled such that throughout the glide the dynamic pressure is kept constant. This is equal to keeping a constant equivalent airspeed. Hence, the gliding vehicle actually executes a quasi-steady flight where the equivalent airspeed and dynamic pressure are kept constant, but the true airspeed decreases when the altitude decreases.

Note that in a real flight, the total time rate of energy dissipation consists of a term accounting for the potential energy and one for the kinetic energy. However, in a steady flight, where the velocity vector is assumed to be constant, the total time rate of energy dissipation is equal to the time rate of the potential energy.

B. Energy-State Approximation

A second (improved) approximation for maximizing range is the energy-state approximation in which it is assumed that the kinetic and potential energy can be exchanged in zero time without loss of total energy [15]. The total energy is considered as the state variable of the system and is continuously decreasing for a gliding vehicle. Differentiating Eq. (18) with respect to time and substituting Eqs. (4) and (9), the time rate of change of the energy height is expressed by

Table 1 Initial conditions and obtained range using $\alpha_{(L/D)\,\max}$

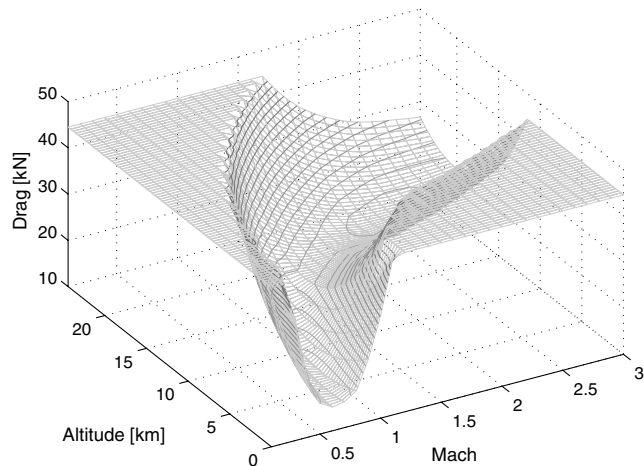| Initial state	V, m/s	h, km	γ, °	E_h, km	M	Range, km
1	108.50	9.40	−29.24	10.00	0.36	32.78
2	171.60	8.50	−14.55	10.00	0.56	34.88
3	228.00	7.35	−17.65	10.00	0.73	33.76
4	583.10	35.00	−10.00	52.51	1.89	134.63
5	661.64	30.00	−10.00	52.51	2.20	136.35
6	732.00	25.00	−10.00	52.51	2.45	130.79

$$\frac{\mathrm{d}E_h}{\mathrm{d}t} = \frac{-VD}{mg} \tag{20}$$

Realizing that $\mathrm{d}s/\mathrm{d}t = V \cos \gamma$, we obtain a relation for the rate of energy dissipation with respect to glide range by dividing Eq. (20) by $\mathrm{d}s/\mathrm{d}t$:

$$\frac{\mathrm{d}E_h}{\mathrm{d}s} = -\frac{D}{mg}\frac{1}{\cos \gamma} \tag{21}$$

The rate at which energy dissipates with glide range is thus proportional to the drag and inversely proportional to the cosine of the flight-path angle. Within the energy-state approximation, where the total energy is considered as a state variable, the maximum range is obtained by minimizing the magnitude of $\mathrm{d}E/\mathrm{d}s$. Assuming that the influence of the flight-path angle is small, the drag has to be constantly minimized for a specific energy height to maximize the range [13,15].
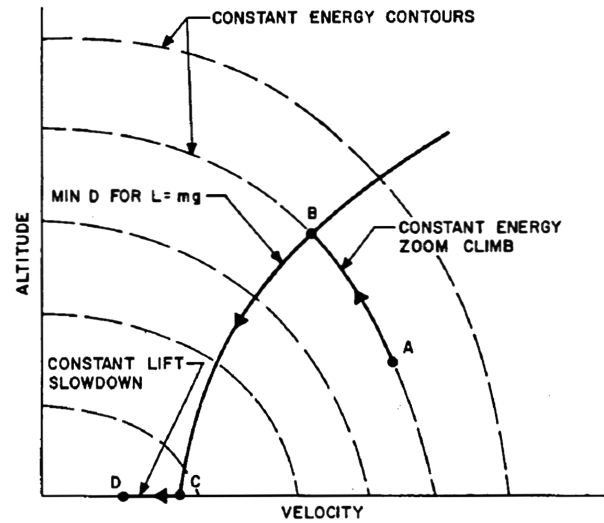
The drag depends on the angle of attack, the altitude, and the velocity. Hence, to be able to plot the drag level in the V, h space or energy space, a specific value for the angle of attack needs to be defined such that the drag becomes a function of only the altitude and the velocity. The angle of attack used is the one required for an equilibrium flight situation (Eqs. (12) and (13), using a zero bank angle σ). The steady-state angle of attack is obtained in the same way as during the calculation of the performance curve. Using the angle of attack for an equilibrium flight situation, the drag level can be calculated for each combination of altitude and velocity. Plotting the drag levels in the energy space indicates contours of constant drag (for $L = W \cos \gamma$). Figure 5 shows a 3-D plot of the contours of constant drag for the supersonic aircraft that was used in [15] to derive the energy-state approximation theory. This figure indicates that for a specific energy level, there is one combination of altitude and velocity for which the drag encountered by the vehicle is a minimum. Hence, a trajectory for which the drag is a minimum at each energy level can be defined in the energy space. Note that the minimum-drag angle of attack for an equilibrium glide condition (where $D = -W \sin \gamma$) is equivalent to the maximum-L/D angle of

attack; both coincide with the minimum-equilibrium-glide flight-path angle.

If the initial conditions are not on this minimum-drag or maximum-range glide path, the vehicle should either zoom-climb or zoom-dive with constant energy to join the curve [13,15]. Figure 6 shows such a typical maximum-range path in the energy space. In the initial phase of flight, an optimal trajectory intercepts the drag valley, after which this valley is followed until a final flare maneuver is performed to extend the range by converting kinetic energy into potential energy. In reality, the zoom-climb or zoom-dive without loss of energy is, of course, not possible for a gliding vehicle, for which the total energy is always decreasing. The drag curves in Fig. 6 are obtained by setting $\cos \gamma = 1$ and using $L = W$. This is a valid approximation for small γ. Because γ can be large for reentry vehicles, $L = W \cos \gamma$ is used for calculating the drag contours for HORUS.

As mentioned in Sec. III.A, the initial subsonic and supersonic conditions and the ranges using $\alpha_{(L/D)\,\max}$ are given in Table 1. Figures 7 and 8 show these trajectories in the energy space (V, h space). The contours of constant drag in the energy space for HORUS are calculated between the maximum-dynamic-pressure boundary and the steady-state stall speed. No contours of constant drag are shown in the transonic speed regime, because the vehicle capabilities in this region are insufficient to have an equilibrium flight situation. A falling motion is performed in the transonic regime [11].

Fig. 6 Sketch of a typical maximum-range glide [15].

Fig. 5 Three-dimensional plot of contours of constant drag for a supersonic aircraft.
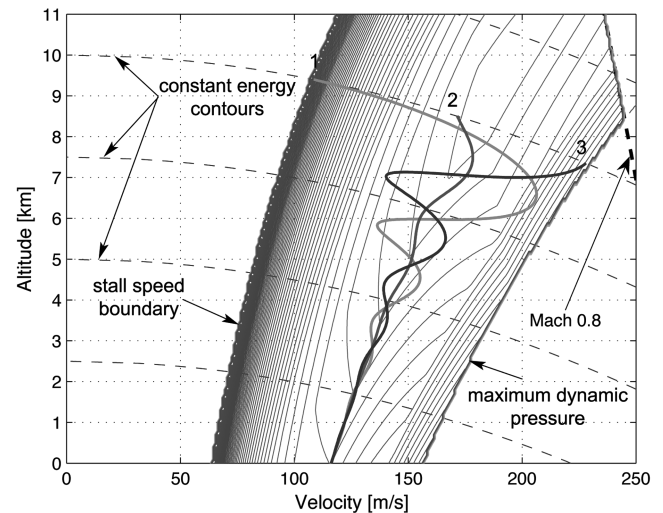
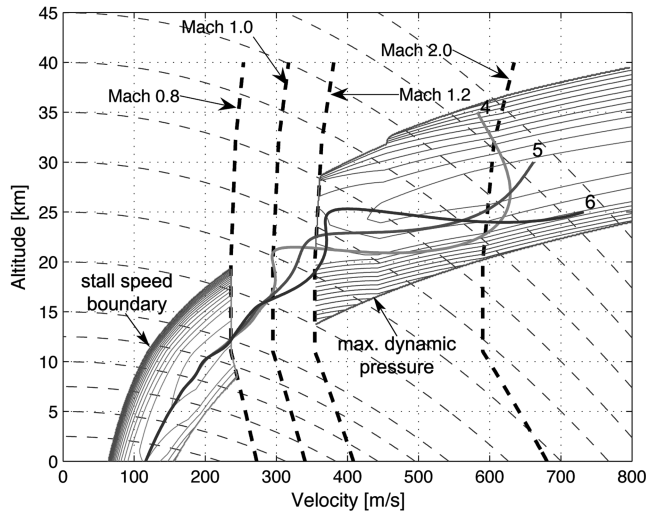**Fig. 7 Subsonic trajectories using $\alpha_{(L/D)\,\max}$.**

Fig. 8 Supersonic trajectories using $\alpha_{(L/D)\,\text{max}}$.

The trajectories using $\alpha_{(L/D)\,\text{max}}$ for the initial subsonic points fluctuate around the drag valley and are damped out near the end of the flight. These oscillations are induced when starting at an initial state (altitude and velocity) away from the drag valley and flying with a constant angle of attack corresponding to maximum L/D (7.5° in the subsonic phase; see Fig. 4). A time-varying angle of attack could improve the trajectory response and prevent the oscillatory behavior. In the case of supersonic initial points, there are no fluctuations when entering the subsonic region, as they have already damped out. In the supersonic region, the fluctuations are also less, because of the lower sensitivity to an offnominal angle of attack.

C. Optimal Trajectories in the Energy Space

The steady-state approximation and energy-state approximation are used to approximate the real optimal solutions. To compare the approximations with the optimal solution, a genetic algorithm (GA) is used as an optimizer to find the optimal control vector (angle of attack) for optimal trajectories in the vertical plane, using the equations of motion given by Eqs. (1–6).

A GA is a global optimizer that mimics nature's own search system, i.e., evolution, to find an optimum [16] and is an easy-to-use tool to explore a design region of interest. The working principle of the GA is based on the principle of survival of the fittest. A GA starts with generating an initial population. Using several operators, such as crossover and mutation, the fittest individuals of the population are chosen to produce offspring. After several generations, the population has evolved into fitter individuals and the evolution is stopped when a predefined stop criterion is met. In this study, the GA is used to optimize a control vector, which represents discrete values of the angle of attack at fixed discrete values of the energy height (the number of nodes was chosen such to balance accuracy and computational load):

approach and landing phase is outside the scope of the current paper. Therefore, for simplicity, it is assumed that the final energy is zero (zero altitude and zero velocity) and the trajectory does not stop at ALI but continues until the vehicle touches the ground (touchdown). Although energy height is chosen as the independent value to specify the angle-of-attack profile, time is used as the independent value during trajectory simulations.

The optimal trajectory problem is subjected to several control-variable and path constraints: α (see Fig. 4), $\dot{\alpha}$ (3°/s), stall speed, and maximum dynamic pressure (e.g., Fig. 7), and maximum load factor (2.5).

The optimal maximum ranges, obtained using the GA, for the same initial points in the V, h space from Table 1 are given in Table 2. These results show that the range can be improved by 3–6% and 1–3% with respect to the subsonic and supersonic $\alpha_{(L/D)\,\text{max}}$ trajectories, respectively.

The resulting subsonic optimal angle-of-attack profiles are given in Fig. 9, together with $\alpha_{(L/D)\,\text{max}}$ (=7.5°). For the largest part of the optimal subsonic maximum-range glide the angle of attack is near $\alpha_{(L/D)\,\text{max}}$, except for the initial and final phases of the flight. Figure 10 shows the corresponding optimized trajectories in the energy space and indicates that the optimal solutions perform initial maneuvers to go the drag valley, follow this drag valley until a final flare maneuver is performed. Comparing this with the trajectories that are obtained using $\alpha_{(L/D)\,\text{max}}$, it can be seen that the optimal trajectories do not show the large fluctuations around the drag valley. Some small fluctuations are still present, because the GA is a global optimizer with less than optimal convergence properties, which usually gives a solution that is only close to the optimal one. Performing a local optimization that uses the result of the GA as an initial guess, would help to eliminate the fluctuations. This is illustrated in Fig. 11, which presents two maximum-range glide trajectories for the supersonic aircraft, as used in [17]. In an attempt to diminish the fluctuations that are present in the optimal solution obtained using the GA, a local Monte Carlo analysis is performed on the optimal α profile. During a Monte Carlo analysis, 1000 new angle-of-attack profiles were randomly calculated and the profile that gives the maximum range has been selected. A new α profile is obtained by taking the α values obtained using the GA at the grid points and additional intermediate points and adding a small random $\Delta\alpha$ value. All the α values are changed at once, but a different random $\Delta\alpha$ is used at each grid point. Figure 11 indicates that fluctuations are diminished using a local optimization after the GA solution. Only in the initial phase of the flight, fluctuations are still present. Although a local optimization can improve the solution, the optimal GA solutions for HORUS as given in Fig. 10 already clearly indicates that the optimal solutions are situated in the drag valley. Despite the small fluctuations, it can be concluded that the energy-state approximation is a valid approximation to the subsonic maximum-range problem of a winged reentry vehicle and an improvement over the steady-state approximation.

As shown in Fig. 12, the obtained optimal solutions for initial supersonic conditions do not follow the drag valley. There are two reasons for this behavior. The first reason can be best observed in

$$E_{h(\text{subsonic})} = [0.0, 1.0, 2.0, 3.0, 4.0, 5.0, 6.0, 7.0, 8.0, 9.0, 10.0, 11.0] \text{ km}$$

$$E_{h(\text{supersonic})} = [0.0, 1.0, 10.0, 15.0, 20.0, 25.0, 30.0, 35.0, 40.0, 45.0, 50.0, 55.0] \text{ km}$$

The first grid is used for subsonic initial states, and the second grid is used for supersonic initial states. Between these discrete values, linear interpolation is used. The energy height was chosen as the independent variable, because for a gliding reentry vehicle it is continuously decreasing, whereas both altitude and velocity can either decrease or increase. Time was also not used, because the time at the end of the TAEM is unknown before the simulation, whereas the energy is supposed to reach a specified value at the ALI. The

trajectories starting above the drag valley and is related to the combination of the vehicle characteristics and the high velocities. The optimal trajectories for the earlier mentioned supersonic aircraft [15] indicate that after a small initial overshoot of the drag valley, the drag valley is followed until the final flare maneuver [17]. However, this vehicle has relative good gliding capabilities with a subsonic and supersonic maximum L/D of 10.3 and 7.6, respectively. However, adapting the original supersonic aircraft aerodynamics such that it
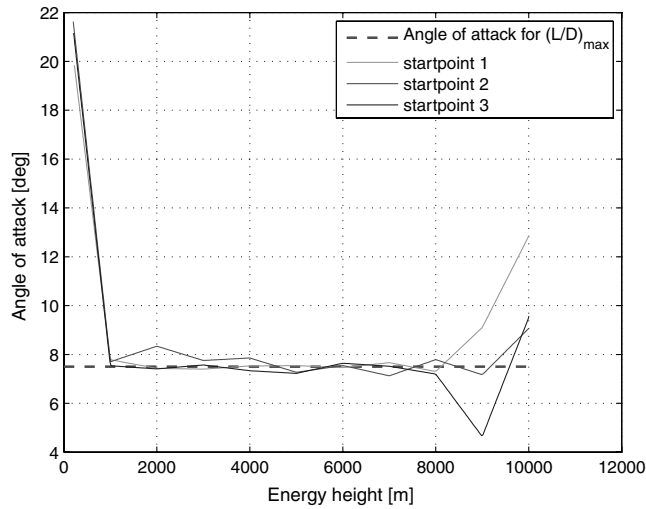
Fig. 9 Optimized subsonic angle-of-attack profiles compared with $\alpha_{(L/D)\,\mathrm{max}}$ (7.5°).
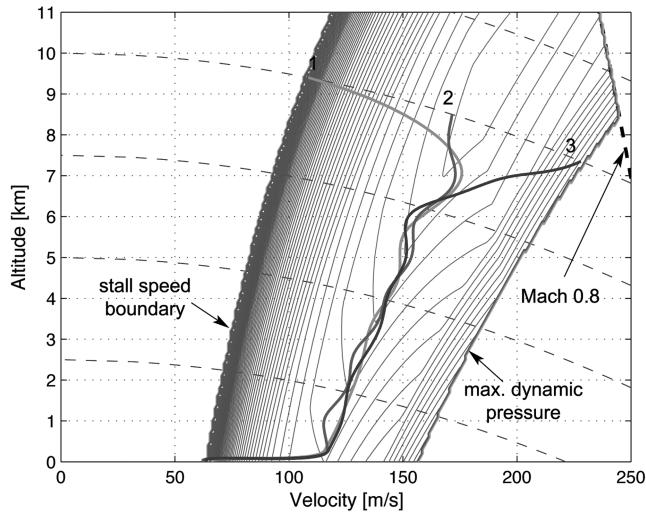

Fig. 10 Subsonic optimal maximum-range solutions.
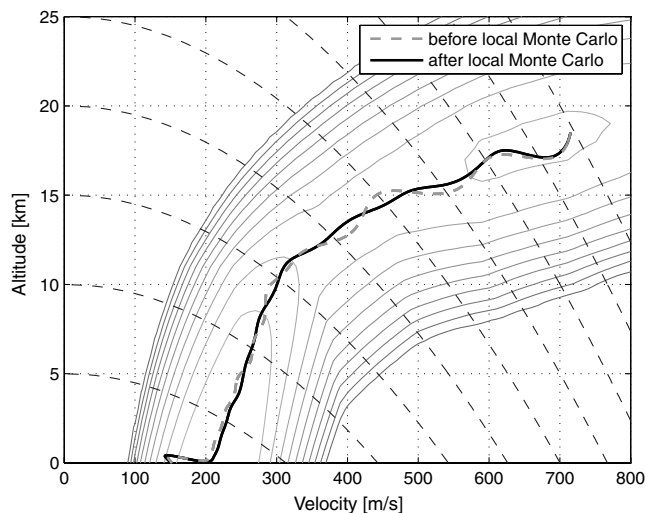

Fig. 11 Maximum-range glide trajectory of supersonic aircraft, before and after local Monte Carlo analysis.
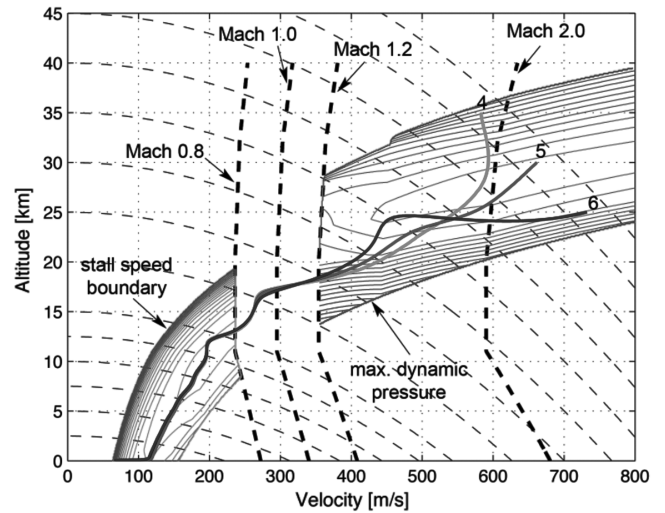

Fig. 12 Supersonic optimal maximum-range solutions.

has a subsonic and supersonic maximum L/D of 4.3 and 3.2, respectively, the optimal trajectories followed by this adapted supersonic aircraft with poor gliding capabilities largely overshoots the drag valley before following the maximum-range path [17]. This confirms the obtained optimal supersonic trajectories of HORUS, which first overshoot the drag valley as it takes too much energy to maneuver and reduce the overshoot. For a supersonic aircraft with relatively good gliding capabilities, these initial overshoots were marginal with respect to the overall trajectory. For vehicles with poor gliding capabilities at subsonic velocities, the overshoots were small. However, when flying at supersonic velocities, the transient maneuvers and overshoots cannot be ignored. The drag encountered during the required pull-up maneuver to follow the drag valley without overshoot is much larger than the drag encountered in the optimal trajectory. As a result, the drag contours calculated using the angle of attack required for equilibrium are no longer valid. However, the general principles of flying at minimum drag for maximum range are still valid, because these maneuvers are conducted at different angles of attack. A second reason for not following the drag valley is the optimal trajectory in the transonic velocity regime. Figure 12 indicates that the three optimal trajectories all start the transonic phase of the flight with the same state conditions in terms of altitude and velocity. In the transonic and subsonic phase, the three trajectories are almost identical. Therefore, it can be concluded that the indicated path through the transonic regime is the optimal solution and the trajectory in the supersonic part is shaped such that the transonic entry point is reached with these optimal conditions.

D. Minimum-Energy Boundary

In the previous sections, questions were answered related to the maximum range that can be achieved, given a specific initial state, but for the purpose of energy management and estimation, it is more valuable to know the minimum amount of energy that is required to fly a specific ground track (range).

It is common to use only one specific value for this minimum-energy height. If the energy state of the vehicle falls below this value, the targeted range cannot be reached [7]. However, both the steady-state solutions and the optimized solutions indicate that although initial points have the same initial energy height, the obtained maximum range is different, as shown in Table 1. The same phenomenon can be observed in Fig. 13, which presents all the initial points (gray area) for which it is possible to fly at least 35.0 km, indicating the minimum required energy, i.e., the maximum-range boundary. If an initial state is situated below the maximum-range boundary (lower energy), it is not possible to reach the target range of 35.0 km, not even with the maximum-range strategy. The figure shows that not all combinations of initial altitude and velocity, with an initial energy height of 10.0 km, will yield a maximum range of at least 35.0 km, as the maximum-range boundary does not follow the
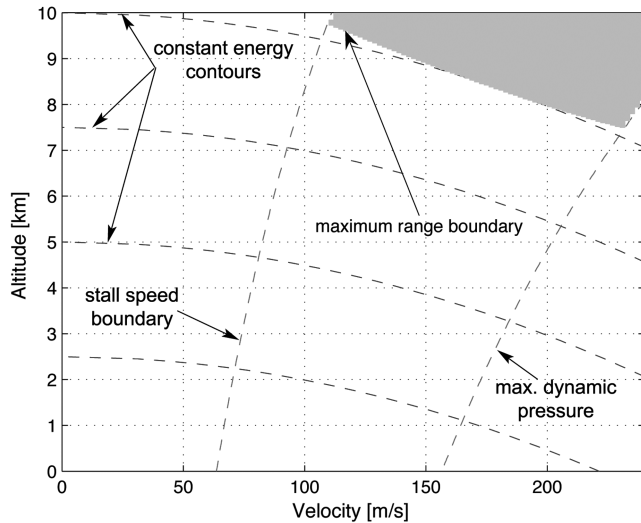
Fig. 13 Combinations of initial altitude and velocity that yield a maximum range of at least 35.0 km (gray area), indicating the maximum-range boundary.

Fig. 14 Optimal maximum-dive trajectory without the use of speed brakes.

lines of constant energy. This is an important observation, because this means that in cases where a guidance system must be able to cope with offnominal conditions, it is not possible to specify only a single minimum-required-energy value for a particular range, for all initial states. Therefore, in addition to specifying the minimum required energy for a specific range, it is also necessary to specify for which combination of altitude and velocity this is valid. The same holds for the maximum-energy boundary, yielding the energy-tube concept. More information on the energy-tube concept and the use in a trajectory planning algorithm can be found in [18].

IV. Maximum-Dive Trajectories in the Vertical Plane

The maximum range is obtained by flying at the smallest flight-path angle and with the lowest amount of drag. Hence, an energy-consuming flight or diving flight is executed at a larger flight-path angle or drag level than during a maximum-range flight. Inspecting the performance curves of HORUS (Fig. 3) and the contours of constant drag in the energy space shows that a larger flight-path angle and drag level can be obtained by flying either at a lower or a higher velocity, depending on whether the angle of attack is higher or lower than that of the maximum L/D. However, when performing a maximum dive, it is natural to lower the nose of the vehicle, and hence many maximum-dive strategies use a flight at maximum dynamic pressure [7–9].

Using the GA, optimal maximum-dive trajectories (minimization of range) are calculated for two subsonic initial points (initial points 1 and 2; see Table 1). The GA searches for the trajectory with the smallest range. Figure 14 shows the obtained optimal-dive trajectories when no speed brakes are used. The maximum dive is obtained by flying at the minimum dynamic pressure or stall-speed boundary and accelerating (by lowering the nose of the vehicle) at the end of the gliding flight. Some fluctuations are present in the optimal diving trajectory for initial point 2. Again, this is due to the fact that the GA is a global optimizer and improvements are still possible.

To explain why the optimal maximum-dive solution is to fly at a minimum dynamic pressure, the drag contours for a steady-state flight situation are also shown in Fig. 14. At the minimum-dynamic-pressure boundary, the encountered drag is higher than when flying at the maximum-dynamic-pressure boundary, due to the high angle of attack (large C_L and C_D). Figure 15 compares the steady-flight situation at a minimum dynamic pressure with the situation at a high dynamic pressure. Although at a minimum dynamic pressure the velocity is smaller, the flight-path angle is larger and the nose is raised above the horizon.

Although the optimal trajectories for a maximum dive indicate that a minimum range is obtained by flying at a minimum dynamic
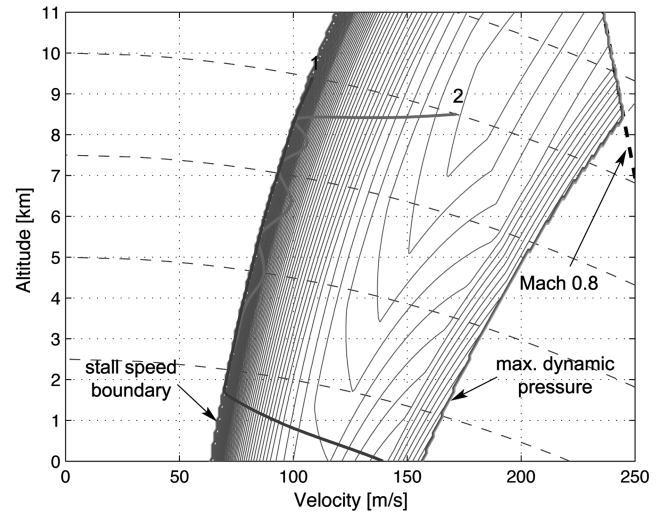
pressure, the authors will still use a maximum dive at maximum dynamic pressure for three reasons:

1) It is the natural instinct to lower the nose of the vehicle and to perform a dive at a high velocity.

2) In the high-nose situation, astronauts do not have a clear view on the ground and the runway as a reference.

3) A disadvantage of flying at a low dynamic pressure is the inherent reduction in control authority, which makes it difficult to reject wind disturbances [9].

It is safer to perform a maximum dive at a high dynamic pressure. However, the solution of flying at minimum dynamic pressure might still be used as a backup in case a dive at maximum dynamic pressure is insufficient.

In [10], a minimum dynamic pressure was used as the reference dynamic pressure to generate optimal TAEM trajectories in the case of effector failures. It is noted that by reducing the velocity, the turn radius can be reduced and hence minimizes the effect of limited bank capabilities in the case of effector failures. Moreover, it is stated that the minimum dynamic pressure is achieved by flying at a relatively shallow flight-path angle, which will tend to extend the overall range of the vehicle [10]. However, this study indicates that for HORUS, flying at a minimum dynamic pressure is performed at a larger flight-path angle and actually reduces the range.
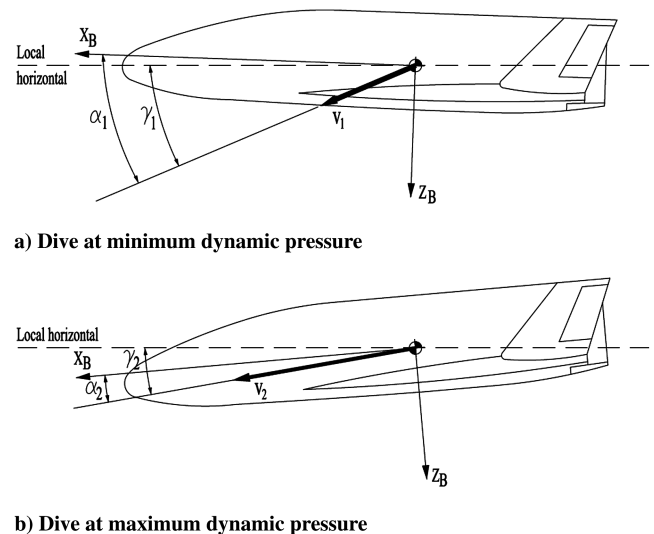

a) Dive at minimum dynamic pressure

b) Dive at maximum dynamic pressure

Fig. 15 Difference between the steady-state dive situation at minimum and maximum dynamic pressure.

V.   Influence of a Turn on the Optimal Trajectories

In several papers [7,9,10], the same reference velocity or dynamic pressure is used for both wings-level and turning flights. In this section, the influence of a turn on the optimal trajectories and reference dynamic pressure is investigated.

In the current study, the optimal-turning problem for a winged reentry vehicle during the terminal area is formulated as follows. Given a HAC with a specific constant radius, what is the optimal longitudinal strategy (angle of attack) such that minimal energy is dissipated during the turn around that specific HAC?

Using the GA, only the angle of attack is optimized for a specific HAC radius, and the required bank angle is calculated by a lateral tracking algorithm. The initial starting point of the flight is situated on the HAC surface, and after turning 270° around the HAC, a straight flight is executed. During this straight flight, a maximum-range flight is performed. Executing a turning flight with minimal energy dissipation means that a maximum amount of energy is still available after the turn. If a wings-level maximum-range flight is performed after the turn, the minimum-energy-dissipation criterion during the turn is transformed into a maximum-range criterion after the turn. Although the initial energy at the start of the turn is known beforehand, it is impossible to know the final energy value at the end of the turn. Hence, the energy cannot be used as the independent variable during the optimal-turn problem. Instead, the heading is used.

After the optimal trajectories are obtained using the GA, an explanation for the shape of these optimal trajectories is obtained using the energy-state approximation. In [13,15], the energy-state approximation is solely used to approximate the maximum-range problem in the vertical plane. In this section, the energy-state approximation is extended to the problem of an optimal turn around a circular HAC. During a turn around a circular HAC with a specific fixed radius, the covered ground-track range is constant. Hence, the optimization criterion of minimum energy dissipation during the HAC can be transformed into a requirement of minimum energy dissipation with respect to range around the HAC: $(dE_h/ds)_{min}$. This criterion is identical to the maximum-range criterion in the energy-state approximation for a wings-level maximum-range flight. Hence, the same methodology can be used in the optimal-turn problem around a HAC. Using Eq. (21) and assuming a small influence of the flight-path angle, the drag has to be minimized during the turn to dissipate the least amount of energy. The banked flight has to be taken into account during the drag calculation, and hence the contours of constant drag must be recalculated for a specific radius of the HAC. The bank angle now has an influence on the required angle of attack for an equilibrium stationary-flight situation [see Eq. (13)]. The larger the bank angle, the larger the required angle of attack (lift) to maintain vertical equilibrium at an equal velocity. Throughout the energy space, different bank angles are required to have a constant HAC radius. For a gliding vehicle, the rate of turn is equal to

$$\dot{\chi} = \frac{V \cos \gamma}{R} \qquad (22)$$

Inserting this definition of the rate of turn in Eq. (14) and rearranging the terms gives

$$\frac{V^2}{R} = \frac{L \sin \sigma}{m \cos^2 \gamma} \qquad (23)$$

Inserting the expression for the lift force and using Eq. (15) gives an expression for the required steady-state bank angle to fly a specific turn radius, which changes with velocity and flight-path angle:

$$\tan \sigma = \frac{V^2 \cos \gamma}{gR} \qquad (24)$$

Figure 16 shows both the resulting optimal-turning trajectories starting at three different initial states (altitude and velocity) for a HAC radius of 5 km, obtained using the GA and the drag contours (5-km-radius HAC) in the energy space. The optimal trajectories are
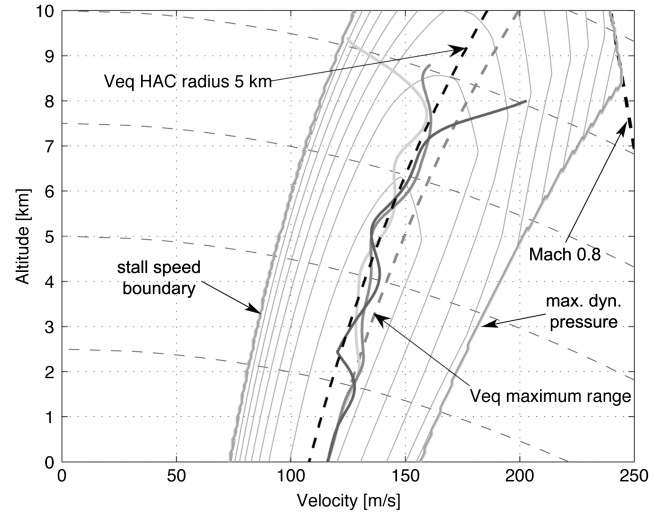

Fig. 16   Contours of constant drag for a HAC with a radius of 5 km and optimal GA trajectories.

situated in the new drag valley for a banked situation and initial maneuvers are performed to intercept the new drag valley. The figure also indicates the equivalent airspeed both in the drag valley for a 5-km-radius HAC and during a maximum-range wings-level flight. The drag valley for the banked situation is shifted to a lower equivalent airspeed with respect to the maximum-range path. Hence, the optimal turn is performed at a lower velocity with respect to the optimal maximum-range velocity. At the end of the turn, a switch is made to the equivalent airspeed of the maximum-range glide. This switch is clearly visible in Fig. 16. A lower velocity during the turn requires a higher angle of attack. Hence, it can be concluded that the optimal turn is performed at a higher angle of attack and a lower velocity.

The radius of the HAC turn has an influence on the optimal trajectories. The smaller the turn radius, the larger the required bank angle. When the radius is decreased, the drag valley is shifted to lower equivalent airspeeds. For a 5-km-radius optimal turn, the optimal equivalent airspeed (equivalent airspeed in the drag valley) is 108.0 m/s, whereas for a turn radius of 4 and 6 km, the optimal values are 104.0 and 112.0 m/s, respectively. The lower the radius, the lower the optimal velocity and the higher the required angle of attack to fly at these lower velocities. Figure 17 shows the steady-state angles of attack in the drag valley as a function of the turn radius and the energy height. The figure confirms that the smaller the turn radius, the higher the optimal angle of attack. These steady-state
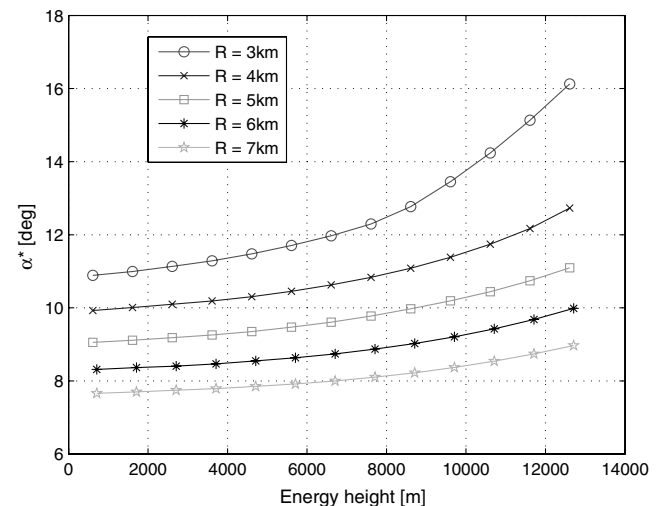

Fig. 17   Open-loop angle of attack as a function of energy height and turn radius for a turn with minimum energy dissipation.

angles of attack will be used in the next section as the open-loop command for the guidance law.

The important conclusion is that the optimal airspeed during a turn is not equal to the optimal airspeed in a straight flight and changes as a function of the turn radius. The smaller the radius, the lower this velocity.

VI.   Guidance Law Design

The calculation of optimal trajectories using a GA is time-consuming. However, using the energy-state approximation, it was possible to detect some general trends in the optimal trajectories. This knowledge is used in this section to design computationally-efficient guidance laws and algorithms to approximate the optimal solutions. For a flight of a reentry vehicle in the terminal area, the maneuvers near the end of the flight, which are present in both the maximum-range and maximum-dive trajectories, are not taken into account.

Considering the maximum-range trajectories, it can be seen from Table 2 that the largest improvement can be obtained in the subsonic flight. For a supersonic flight, the steady-state assumption and the simple fixed angle-of-attack profile (Fig. 4) yield a good approximation. The possible marginal improvements do not justify a more complicated guidance law at this stage. The turn around the HAC is performed in the subsonic region. During this subsonic turn, large improvements can be obtained, since the optimal velocity changes with turn radius. Hence, the design of a guidance law for a subsonic maximum-range flight and the changes required during an optimal subsonic turning flight are described in this section.

A.   Subsonic Maximum-Range Guidance Law

The optimal strategy for a subsonic maximum-range flight is to glide toward the drag valley (or the required dynamic pressure) and then maintain this dynamic pressure throughout the gliding flight. Depending on the initial state with respect to the drag valley, a different optimal glide toward the drag valley and optimal maneuvers to intercept this valley will result, such that all optimal trajectories have a different optimal dynamic pressure profile. Hence, it is not possible to use only a single reference dynamic pressure profile if the maximum range must be calculated for different initial states. The most accurate, but also the most difficult solution is to use a dynamic pressure tracking scheme in combination with an onboard algorithm that calculates the complete optimal reference dynamic pressure profile, including the optimal maneuvers, based on the current initial conditions.

In the current study, a simpler approximation is used. The constant dynamic pressure value in the drag valley (8242 N/m^2) is used as a reference, since this dynamic pressure value is constant for all subsonic wings-level maximum-range problems. The tracking of this reference is done by a simple guidance law for the vertical motion, which regulates the angle of attack:

$$\alpha = \alpha^* + K_p(\bar{q}_{\text{ref}} - \bar{q}) + K_d \dot{\bar{q}} \qquad (25)$$

where α^* is an open-loop reference angle of attack required to have an equilibrium flight situation at the required dynamic pressure and the current energy height ($\alpha^* = 7.5°$; see Figs. 4 and 9), and $\bar{q}_{\text{ref}}$ is the optimal constant reference value. The vertical guidance law is a
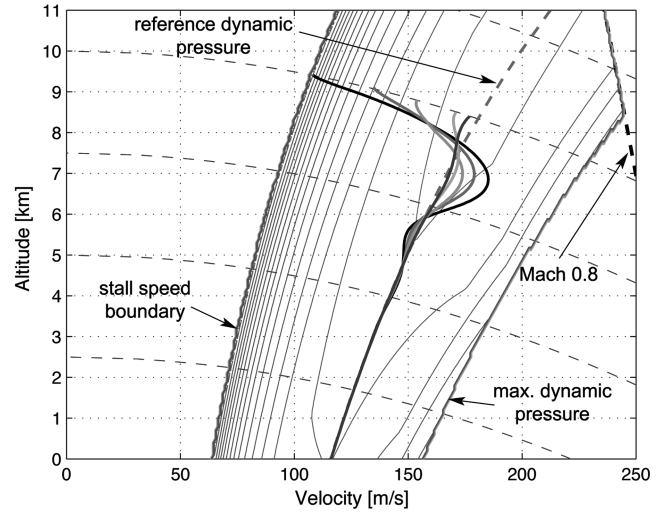

Fig. 18   Suboptimal trajectories in the energy space for initial states with $q_{\text{ini}} < q_{\text{ref}}$, using robust design.

so-called proportional–derivative control law. The optimal transient maneuvers to intercept the drag valley are now contained in the gain values K_p and K_d. Changing the gains results in different responses and thus different trajectories. Hence, optimal gains must be calculated that resemble the optimal transient maneuvers as closely as possible. A GA is again used as an optimizer to calculate the optimal values for gains, once more using the equations of motion given by Eqs. (1–6). For a single specific initial state, it is possible to calculate values for the gains, which result in a good approximation of the real optimal trajectories (range differences of 0.3%). However, it is not possible to use the same set of gains for a different initial state, because it results in a trajectory that does not follows the drag valley correctly. Therefore, a different initial state requires a different set of optimal gains. However, for a further analysis of the energy estimation and the required longitudinal guidance strategies, it seems wise to have only one simple set of gains that can be used for all subsonic initial states, rather than a complex system.

A practical solution is the use of a robust-design method. The purpose of using robust design is to find a single set of optimal gains such that the system performs well under all conditions. Although the obtained gains are suboptimal if the resulting trajectories for each specific initial state are considered separately, an acceptable optimal global performance is obtained with a single set of gains. For each of the initial states in the energy space shown in Figs. 18 and 19, the obtained ranges are 0.8% less than for the real optimal trajectories. This is a less accurate approximation than if the gains are optimized for a specific initial state (only 0.3% less range), but it is still a better approximation than using $\alpha_{(L/D)\,\text{max}}$ (range differences of 3%). The suboptimal set of gains is obtained by simultaneously optimizing a single set of gains for several initial states.

Table 2   Obtained maximum optimal range for HORUS and improvement with respect to steady-state solution

Initial state	Range α_{optimal}, km	Improvement, %
1	34.87	6.38
2	35.97	3.13
3	35.18	4.21
4	138.93	3.19
5	138.80	1.80
6	132.95	1.65

Table 3   Suboptimal gains for subsonic maximum range resulting from robust design; $\Delta q = q_{\text{ref}} - q_{\text{initial}}$

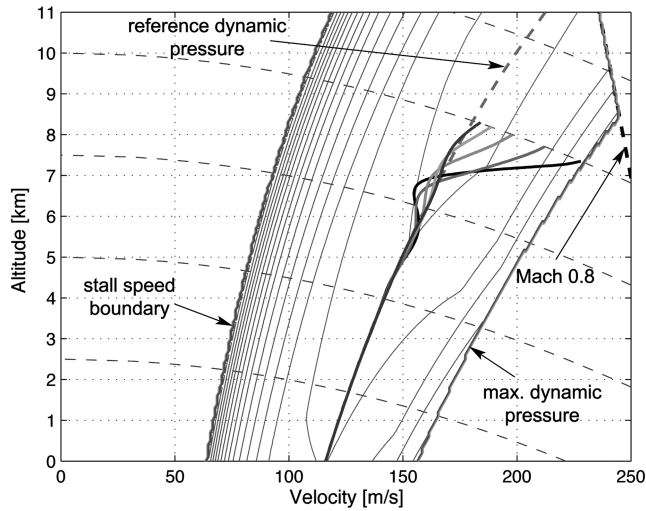| Δq, Pa	K_p, deg /Pa	K_d, (deg ·s)/Pa
Set 1		
>5000	0.001015	−0.002906
5000 to 3000	0.000478	0.003800
3000 to 1500	0.000591	0.002438
1500 to 500	−0.000171	0.003850
<500	−0.000027	0.003862
Set 2		
> − 500	−0.000188	0.003825
−1500 to −500	0.000206	0.003613
−3000 to −1500	0.000385	0.003999
−5000 to −3000	0.000368	0.003092
< − 5000	0.000045	−0.000288

Fig. 19 Suboptimal trajectories in the energy space for initial states with $q_{ini} > q_{ref}$, using robust design.

The type of transient maneuvers required to intercept the drag valley differ for initial states with a lower or a higher initial dynamic pressure than the reference dynamic pressure in the drag valley. Hence, the method of robust design is applied separately to these two regions of initial states. Rather than using a single value for the K_p and K_d throughout the complete flight, five values are used, depending on the current dynamic pressure (gain scheduling). Both in the case of lower or higher initial dynamic pressures, five initial states with the same initial energy height, but with a different dynamic pressure, are used to define the single suboptimal set of gains. Using the robust-design method, the GA optimizes the total maximum range for the five initial states, yielding the 10 gain values. Table 3 presents the obtained suboptimal set of gains. If the initial dynamic pressure is lower than the reference dynamic pressure, set 1 must be used, and when it is larger, set 2.

Figures 18 and 19 show the suboptimal trajectories obtained using the single suboptimal set of gains for five initial states in the region with a dynamic pressure lower than the reference dynamic pressure and in the region with a higher dynamic pressure, respectively. The suboptimal sets of gains are calculated for initial states with an identical initial energy height of 10.0 km. However, Fig. 20 indicates that the guidance law is also valid for other initial states. Maximum-range trajectories are shown for initial states with an altitude between
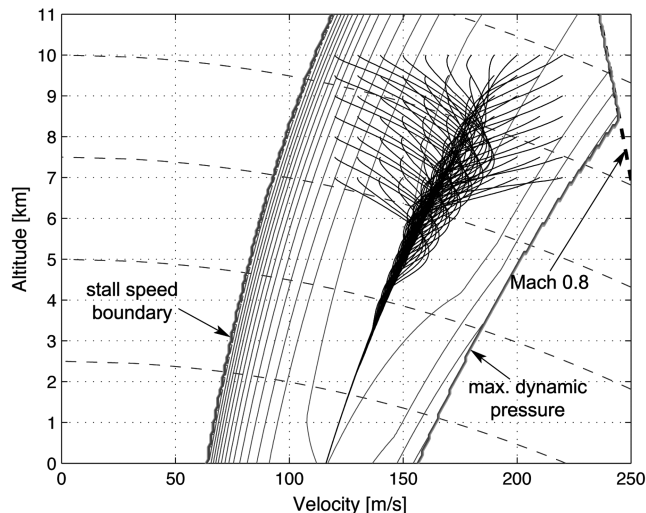

Fig. 20 Suboptimal trajectories in the energy space for initial states with a different initial energy. Gains obtained from robust design (Table 3) are used to calculate the trajectories.
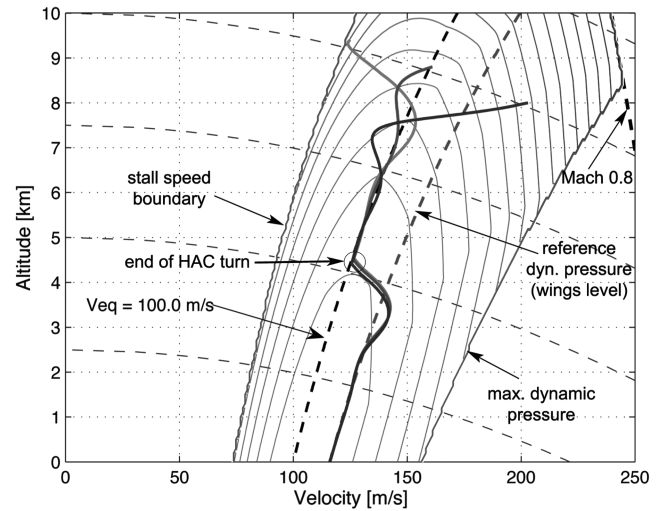

Fig. 21 Trajectories in the energy space using a longitudinal guidance law and the optimal gains resulting from the robust-design analysis, for a HAC radius of 3 km.

7.0 and 10.0 km and with a velocity between 115.0 and 220.0 m/s. Using a single set of gains for different initial states, all the maximum-range trajectories track the drag valley. The gains used for calculating these trajectories are given in Table 3.

B. Subsonic Optimal-Turn Guidance Law

The set of suboptimal gains as given in Table 3 is still valid for an optimal-turning flight, in combination with the guidance law as given by Eq. (25). Figure 21 shows three resulting trajectories in the energy space for a subsonic turning flight around a HAC of 3 km. The optimal reference equivalent airspeed in the drag valley for this turn radius is 100.0 m/s (optimal equivalent airspeeds for other turn radii are given in Sec. V). This figure indicates that the suboptimal gains resulting from the robust-design method are still able to intercept the reference dynamic pressure in a turn, for different initial states. After a turn of 270°, the bank angle is reduced to 0° and the dynamic pressure for a wings-level maximum-range flight is intercepted.

Although the suboptimal gains can still be used, two remarks must be made. The open-loop steady-state angle of attack α^* is no longer a constant. It changes as a function of both the energy height and turn radius. As shown in Fig. 17, the smaller the turn radius, the higher the steady-state angle of attack. Note that the required steady-state angle of attack required to fly a specific turn radius depends on the altitude and the velocity. However, during an optimal turn around a specific HAC radius, it was shown that the vehicle needs to follow the drag valley (constant equivalent airspeed or dynamic pressure). Therefore, there is only one cross point of each energy height with the optimal equivalent airspeed resulting in only one optimal combination of altitude and velocity at each energy height. Hence, it is sufficient to specify the angle of attack as a function of the energy height. A second remark is related to high-bank situations. When the vehicle is banked close to its limits (60°), deviations from the reference dynamic pressure can occur during the turn. Because of the extreme banked situation, a falling motion occurs. The longitudinal guidance law should calculate a larger angle of attack to increase the lift force to prevent the falling motion. The current gains are not sufficient to increase the angle of attack. This phenomenon can be seen especially at small turn radii. However, this situation occurs only rarely and only lasts shortly until the bank angle is lowered again. Overall, the obtained gains perform well.

VII. Conclusions

Although it is common to use the angle-of-attack profile for a maximum lift-to-drag ratio as the maximum-range strategy, this paper shows that a larger range can be obtained by using a different strategy. The energy-state approximation states that the optimal

strategy to perform a subsonic maximum-range flight is to fly with minimum drag, which is confirmed by numerical optimization using a genetic algorithm, despite the vehicle's poor gliding capabilities. If the vehicle starts at an initial state that is not located on this path, transient maneuvers are performed to intercept the maximum-range glide path. However, in the case of a supersonic maximum-range flight, the energy-state approximation (using an equilibrium condition) is no longer valid, because the drag encountered during the transient maneuvers is too large. The general principles of dissipating the least amount of energy with respect to range and flying at minimum drag is still valid.

Significant improvements (3–6%) in range can be obtained for a subsonic maximum-range flight using the optimal strategies, compared with the trajectories using $\alpha_{(L/D)\max}$. Only minor improvements are obtained during a supersonic flight (1–3%). Hence, the angle-of-attack profile for $L/D_{\max}$ is used for a supersonic maximum-range flight, and for a subsonic maximum-range flight, the longitudinal strategy is to track the reference dynamic pressure in the drag valley. This leads to acceptable deviations from the optimal ranges.

An optimal subsonic turn (one that minimizes energy loss) is performed at a larger angle of attack and at a lower velocity than during a subsonic wings-level maximum-range flight. The smaller the radius, the lower the optimal velocity and the larger the required angle of attack. The energy-state approximation is valid for the optimal-turning problem. The drag valley is different for different turn radii and is shifted to lower dynamic pressures as the turn radius decreases.

The optimal dive (one that minimizes range and maximizes energy loss) is obtained by flying along a minimum-dynamic-pressure profile close to the stall boundary, because this yields the largest encountered drag. The energy-state approximation indicates that the drag encountered at the minimum-dynamic-pressure boundary is larger than at the maximum-dynamic-pressure boundary. When the inherent reduction in control capabilities is too large at this minimum dynamic pressure, a dive near maximum dynamic pressure should be considered.

An important conclusion from all the optimal trajectories is that the optimal dynamic pressure profiles, especially the initial transient parts, change for different initial states. A different initial state requires a different optimal dynamic pressure profile, if the complete flight is considered. Hence, it is not possible to use a single fixed dynamic pressure profile in the case of offnominal conditions.

Although it is common to specify a single value for the minimum required energy that is needed to reach a specific ground-track range using the maximum-range strategy, simulations indicate that the maximum range differs for initial states with the same initial energy. Therefore, in addition to the minimum energy height it is also necessary to specify for which combination of kinetic and potential energy this is valid.

References

[1] Branscome, D. R., and Reese, T. G., "NASA Launch Vehicles: The Next 20 Years," *Acta Astronautica*, Vol. 21, 1990, pp. 243–253.
doi:10.1016/0094-5765(90)90047-O

[2] Darwin, C. R. Austin, G., Varnado, L., and Eudy, G., "A View Toward Future Launch Vehicles: A Civil Perspective," *Acta Astronautica*, Vol. 25, 1991, pp. 165–175.
doi:10.1016/0094-5765(91)90144-T

[3] Feustel-Büechl, Isakeit, D., and Pfeffer, H., "Wings for European Spaceflight—The Future of Space Transportation," *ESA Bulletin*, No. 66, 1991, pp. 21–28.

[4] Hanson, J., "New Guidance for New Launchers," *Aerospace America*, March 2003, pp. 36–41.

[5] Moore, T. E., "Space Shuttle Entry Terminal Area Energy Management," NASA TM-104744, Nov. 1991.

[6] Kluever, C. A., and Horneman, K. R., "Terminal Trajectory Planning and Optimization for an Unpowered Reusable Launch Vehicle," AIAA Guidance, Navigation, and Control Conference, AIAA Paper 2005-6058, Aug. 2005.

[7] Büchner, T., "Trajectory Generation Strategy for the Terminal Area of a Reusable Launch Vehicle," International Astronautical Congress, Paper 03-W.1.06, 2003.

[8] Da Costa, R. R., "Studies for Terminal Area GNC of Reusable Launch Vehicles," AIAA Guidance, Navigation, and Control Conference, AIAA Paper 2003-5438, Aug. 2003.

[9] Hull, J., Gandhi, N., and Shierman, J., "In Flight TAEM/Final Approach Trajectory Generation for Reusable Launch Vehicles," Infotech@ Aerospace, AIAA Paper 2005-7114, Sept. 2005.

[10] Kluever, C. A., "Terminal Guidance for an Unpowered Reusable Launch Vehicle with Bank Constraints," *Journal of Guidance, Control, and Dynamics*, Vol. 30, No. 1, 2007, pp. 162–168.
doi:10.2514/1.24864

[11] Helmersson, A., "Terminal Area Guidance Strategies," Messerschmitt-Bölkow-Blohm, TN-ESA 6718/85-8, 1988.

[12] Mooij, E., "Aerospace-Plane Flight Dynamics. Analysis of Guidance and Control Concepts," Ph.D. Dissertation, Delft University of Technology, Delft, The Netherlands, 1998.

[13] Vinh, N. X., *Optimal Trajectories in Atmospheric Flight*, Elsevier, New York, 1981.

[14] Mooij, E., "The HORUS-2B Reference Vehicle," Memo. m-692, Delft University of Technology, Faculty of Aerospace Engineering, Delft, The Netherlands, 1995.

[15] Bryson, A. E., Desai, M. N., and Hoffman, W. C., "The Energy-State Approximation in Performance Optimization of Supersonic Aircraft," AIAA Paper 68-877, Aug. 1968.

[16] Michalewicz, Z., *Genetic Algorithms + Data Structures = Evolution Programs*, 3rd ed., Springer–Verlag, Berlin, 1996.

[17] De Ridder, S., and Mooij, E., "Optimal Terminal-Area Strategies and Energy-Tube Concept for a Winged Re-Entry Vehicle," AIAA Paper 2009-5769, Aug. 2009.

[18] De Ridder, S., and Mooij, E., "Terminal Area Trajectory Planning Using the Energy-Tube Concept for Reusable Launch Vehicles," *Acta Astronautica*, Vol. 68, Nos. 7–8, April–May 2011, pp. 915–930.
doi:10.1016/j.actaastro.2010.08.032